Chemical Physics 462 (2015) 71–78

Contents lists available at ScienceDirect

Chemical Physics

journal homepage: www.elsevier.com/locate/chemphys

Mutual vibrational quenching in CO + H_2 collisions

Robert C. Forrey [a,*], B.H. Yang [b], P.C. Stancil [b], N. Balakrishnan [c]

[a] Department of Physics, Penn State University, Berks Campus, Reading, PA 19610-6009, United States
[b] Department of Physics and Astronomy and the Center for Simulational Physics, University of Georgia, Athens, GA 30602, United States
[c] Department of Chemistry, University of Nevada Las Vegas, Las Vegas, NV 89154, United States

ARTICLE INFO

Article history:
Available online 3 August 2015

Keywords:
Molecular data
Inelastic processes
Quantum dynamics

ABSTRACT

Vibrational quenching of CO and H_2 is studied quantum mechanically for collisions where both molecules are vibrationally excited. A five-dimensional (5D) coupled states (CS) approximation is used to formulate the dynamics. The approximation is tested against six-dimensional (6D) results for CO + H_2 with single vibrational excitation using both the CS approximation and the full close-coupling (CC) method. The 5D approximation is shown to provide a practical and reliable numerical approach for obtaining state-to-state cross sections in the computationally challenging case of mutual rovibrational de-excitation. State-resolved and partially-summed cross sections are presented for this astrophysically important collision system over a wide range of energies, and prospects for developing a database of rovibrational quenching rate coefficients are discussed.

1. Introduction

Vibrational quenching of carbon monoxide in collisions with molecular hydrogen has been studied for more than 50 years [1–6]. H_2 and CO are the most abundant molecular species in the majority of interstellar environments and have been the focus of countless astrophysical studies and observations. When these environments are irradiated with an intense UV field, the radiation drives the chemistry and internal level populations out of equilibrium, and it is necessary to account for the detailed excitation and de-excitation mechanisms of both molecules [7,8]. An example where such detailed information is needed is a photodissociation region (PDR) which resides at the interface of hot HII (ionized hydrogen) and cold molecular regions. Various astrophysical simulation packages that model the physics and chemistry of PDRs have been developed [9–13] which account for excitation mechanisms of both H_2 and CO. Other examples where CO molecules have been detected include cometary comae in our solar system [14], the atmospheres of extrasolar giant planets [15], and objects as distant as high redshift quasars [16]. Because the ratio of CO to H_2 is roughly constant in dense molecular gas, the observed CO abundance is often used to estimate the abundance of H_2. Therefore, a reliable database of state-to-state rate coefficients is critical to interpreting the spectra from a variety of astrophysical environments. In particular, high-resolution observations of star-forming regions and protoplanetary disks of young stellar objects have shown evidence of rovibrational transitions for states where rate coefficients are currently lacking. In order to model such environments, current simulations have relied on approximate scaling methods which are known to be unreliable [17,18].

Recent progress [19] in full six-dimensional (6D) quantum dynamics of CO + H_2 have achieved unprecedented agreement with experiment for the de-excitation of vibrationally excited CO when H_2 is vibrationally unexcited. These calculations represent initial steps towards the goal of obtaining the CO + H_2 vibrational relaxation data needed for astrophysical modeling. The key to developing a reliable database is the use of an accurate potential energy surface (PES) together with an accurate treatment of the dynamics. Previous studies [20–23] consisting of 4D dynamical calculations with various combinations of angular momentum decoupling approximations yielded results for the vibrational quenching of CO which varied by more than two orders of magnitude [19]. The large dispersion for the previous calculations was due to a combination of reduced dimensionality and decoupled angular momentum which made it difficult to assess the reliability of each approximation. These uncertainties were eliminated [19] by utilizing a full-dimensional PES and a numerically exact close-coupling (CC) formulation which combines 6D dynamics and full angular-momentum coupling. The theoretical rate coefficients computed using this approach yielded results in close agreement with available experimental data for this system [4–6].

The present work aims to extend these initial calculations to include collisions where H_2 is also vibrationally excited. Ideally,

* Corresponding author.
E-mail address: rcf6@psu.edu (R.C. Forrey).

http://dx.doi.org/10.1016/j.chemphys.2015.07.001
0301-0104/

the dynamical description would use the same 6D-CC formulation used in the singly vibrationally excited case. Such calculations, however, require substantially enlarged basis sets to account for the added vibrational flexibility and would not be feasible at this time due to practical considerations. For example, when the basis set for H_2 was restricted to its lowest vibrational state, the calculated cross sections consumed more than 40,000 CPU hours and used approximately 0.5 TB of disk space per partial wave [19]. Adding vibrational flexibility into the H_2 basis set would dramatically increase these already high computational demands to the point where it would be practically impossible to bring such calculations to completion. In such cases, it is desirable to use a dynamical decoupling approximation, but one which captures the most important physics.

One of the best methods for decoupling orbital angular momentum is the coupled states or centrifugal sudden (CS) approximation [24–26]. The CC and CS formulations have both been developed for diatom–diatom systems [27–29] and a comparison of the two formulations was recently given for $H_2 + H_2$ in full dimensionality [30]. In the present work, we investigate the possibility of using the CS approximation to describe the dynamics of $CO + H_2$ collisions. Two versions of the CS approximation are considered. The first version corresponds to full 6D dynamics with no additional approximations beyond the usual orbital angular momentum decoupling. This approach is computationally less demanding than a 6D-CC calculation, however, it still requires significant computational resources due to the large number of rotational states in the CO molecule that are coupled to the rotational states of H_2. In order to achieve additional computational savings, a second version of the CS approximation is investigated which corresponds to 5D dynamics. This version maintains the vibrational degrees of freedom for both diatoms but assumes the twist-angle dependence of the PES is negligible, which leads to conserved values for the individual molecule angular momentum projection quantum numbers. The 5D-CS and 6D-CS approximations are tested against the 6D-CC formulation, and new results are given for mutual vibrational quenching.

2. Theory

The quantum mechanical CC and CS formulations for diatom–diatom collisions have been given previously [27–29]. In order to make clear the distinctions between the 5D and 6D formulations, we provide a brief overview of the theory. The Hamiltonian of the four-atom system is given by

$$H(\vec{r}_1,\vec{r}_2,\vec{R}) = T(\vec{r}_1) + T(\vec{r}_2) + T(\vec{R}) + V(\vec{r}_1,\vec{r}_2,\vec{R}). \tag{1}$$

The radial kinetic energy term $T(\vec{R})$ describes the center-of-mass motion, and the terms $T(\vec{r}_1)$ and $T(\vec{r}_2)$ represent the kinetic energies of the CO and H_2 molecules, respectively. The potential energy for the four-body system is given by

$$V(\vec{r}_1,\vec{r}_2,\vec{R}) = U(\vec{r}_1,\vec{r}_2,\vec{R}) + V(\vec{r}_1) + V(\vec{r}_2), \tag{2}$$

where $V(\vec{r}_1)$ and $V(\vec{r}_2)$ are the two-body potential energies of the isolated CO and H_2 molecules, and $U(\vec{r}_1,\vec{r}_2,\vec{R})$ is the four-body interaction potential which vanishes at large separations. The 6D Jacobi coordinate system in Fig. 1 is used where R is the distance between the centers-of-mass of the diatomic molecules, θ_1 is the angle between $\vec{r}_1$ and $\vec{R}$, θ_2 is the angle between $\vec{r}_2$ and $\vec{R}$, and ϕ is the out-of-plane dihedral angle or "twist" angle. The interaction potential may be expanded as

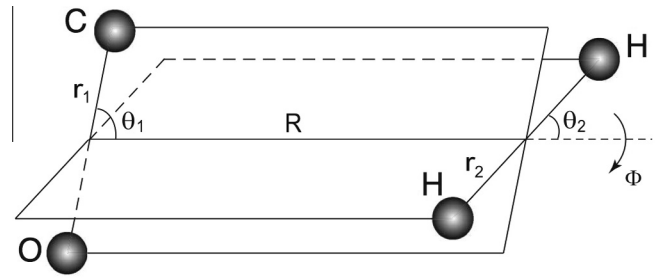

Fig. 1. Six-dimensional Jacobi coordinates for CO-H_2. R is the distance between the centers of mass of CO and H_2, r_1 and r_2 are bond lengths, θ_1 and θ_2 are the respective angles between $\vec{R}$ and $\vec{r}_1$ and $\vec{r}_2$, and ϕ is the dihedral or twist angle.

$$U(\vec{r}_1,\vec{r}_2,\vec{R}) = \sum_{\lambda_1,\lambda_2,\lambda_{12}} A_{\lambda_1,\lambda_2,\lambda_{12}}(r_1,r_2,R)\, Y_{\lambda_1,\lambda_2,\lambda_{12}}(\hat{r}_1,\hat{r}_2,\hat{R}) \tag{3}$$

with

$$Y_{\lambda_1,\lambda_2,\lambda_{12}}(\hat{r}_1,\hat{r}_2,\hat{R}) = \sum_{all\ m} \langle \lambda_1 m_{\lambda_1} \lambda_2 m_{\lambda_2} | \lambda_{12} m_{\lambda_{12}} \rangle\, Y_{\lambda_1 m_{\lambda_1}}(\hat{r}_1)\, Y_{\lambda_2 m_{\lambda_2}}(\hat{r}_2)\, Y^*_{\lambda_{12} m_{\lambda_{12}}}(\hat{R}), \tag{4}$$

where $\langle \ldots | \ldots \rangle$ represents a Clebsch-Gordan coefficient and $Y_{\lambda m}(\hat{r})$ is a spherical harmonic. The total wave function for the four-atom system is expanded in terms of a diabatic basis set which contains products of molecular wave functions $\chi_{v_i j_i}(r_i)$ with vibrational and rotational quantum numbers v_i and j_i, respectively. To compact the notation, we define $v \equiv v_1 v_2$ and $j \equiv j_1 j_2$, so that the basis functions may be written as

$$\chi_{vj}(r_1,r_2) = \chi_{v_1 j_1}(r_1)\chi_{v_2 j_2}(r_2). \tag{5}$$

The radial interaction potential matrix elements are obtained by integrating over the internal coordinates

$$B^{\lambda_1,\lambda_2,\lambda_{12}}_{vj;v'j'}(R) = \int_0^\infty \int_0^\infty \chi_{vj}(r_1,r_2) A_{\lambda_1,\lambda_2,\lambda_{12}}(r_1,r_2,R)\chi_{v'j'}(r_1,r_2) r_1^2 r_2^2 dr_1 dr_2. \tag{6}$$

The full potential matrix depends on the scattering formulation. For the CC method, the channels are defined by the index $n \equiv \{v, j, j_{12}, l\}$, where l is the orbital angular momentum quantum number and $\vec{j}_{12} = \vec{j}_1 + \vec{j}_2$. The total angular momentum quantum number J is defined by $\vec{J} = \vec{l} + \vec{j}_{12}$, and the potential matrix for 6D-dynamics is given by

$$\begin{aligned} V^J_{n;n'}(R) = (4\pi)^{-3/2} \sum_{\lambda_1,\lambda_2,\lambda_{12}} & (-1)^{j'_1+j'_2+j_{12}+J} \\ & \times \left([j_1][j_2][j_{12}][l][j'_1][j'_2][j'_{12}][l'][\lambda_1][\lambda_2][\lambda_{12}]^2\right)^{1/2} \\ & \times \begin{pmatrix} l' & \lambda_{12} & l \\ 0 & 0 & 0 \end{pmatrix} \begin{pmatrix} j'_1 & \lambda_1 & j_1 \\ 0 & 0 & 0 \end{pmatrix} \begin{pmatrix} j'_2 & \lambda_2 & j_2 \\ 0 & 0 & 0 \end{pmatrix} \\ & \times \begin{Bmatrix} l & l' & \lambda_{12} \\ j'_{12} & j_{12} & J \end{Bmatrix} \begin{Bmatrix} j_{12} & j_2 & j_1 \\ j'_{12} & j'_2 & j'_1 \\ \lambda_{12} & \lambda_2 & \lambda_1 \end{Bmatrix} B^{\lambda_1,\lambda_2,\lambda_{12}}_{vj;v'j'}(R) \end{aligned} \tag{7}$$

which is diagonal with respect to J and independent of M, the projection of $\vec{J}$ in the space-fixed frame. The notations $(===)$, $\{===\}$, and $\{\equiv\equiv\equiv\}$ are the usual 3j, 6j, and 9j symbols, and $[j] = (2j+1)$. For the CS formulation, the index $n \equiv \{v, j, j_{12}\}$ and the potential matrix for 6D-dynamics is given by

$$V^{\Omega}_{n;n'}(R) = (4\pi)^{-3/2} \sum_{\lambda_1,\lambda_2,\lambda_{12}} (-1)^{j'_1+j'_2+j'_{12}+\Omega} \times \left([j_1][j_2][j_{12}][j'_1][j'_2][j'_{12}][\lambda_1][\lambda_2][\lambda_{12}]^2\right)^{1/2} \times \begin{pmatrix} j'_1 & \lambda_1 & j_1 \\ 0 & 0 & 0 \end{pmatrix} \begin{pmatrix} j'_2 & \lambda_2 & j_2 \\ 0 & 0 & 0 \end{pmatrix} \begin{pmatrix} j'_{12} & \lambda_{12} & j_{12} \\ \Omega & 0 & -\Omega \end{pmatrix} \times \begin{Bmatrix} j_{12} & j_2 & j_1 \\ j'_{12} & j'_2 & j'_1 \\ \lambda_{12} & \lambda_2 & \lambda_1 \end{Bmatrix} B^{\lambda_1,\lambda_2,\lambda_{12}}_{vj;v'j'}(R) \tag{8}$$

which is independent of J and diagonal with respect to Ω, the projection of $\vec{J}$ on the body-fixed z-axis, which is taken to lie along the direction of $\vec{R}$. For the CS formulation with no twist-angle dependence, the index $n \equiv \{v,j\}$ and the potential matrix for 5D-dynamics is

$$V^{m_1,m_2}_{n;n'}(R) = (4\pi)^{-3/2} \sum_{\lambda_1,\lambda_2,\lambda_{12}} (-1)^{\lambda_1+\lambda_2+m_1+m_2} \times \left([j_1][j_2][j'_1][j'_2][\lambda_1][\lambda_2][\lambda_{12}]^2\right)^{1/2} \times \begin{pmatrix} j'_1 & \lambda_1 & j_1 \\ 0 & 0 & 0 \end{pmatrix} \begin{pmatrix} j'_2 & \lambda_2 & j_2 \\ 0 & 0 & 0 \end{pmatrix} \begin{pmatrix} j'_1 & \lambda_1 & j_1 \\ -m_1 & 0 & m_1 \end{pmatrix} \times \begin{pmatrix} j'_2 & \lambda_2 & j_2 \\ -m_2 & 0 & m_2 \end{pmatrix} \begin{pmatrix} \lambda_1 & \lambda_2 & \lambda_{12} \\ 0 & 0 & 0 \end{pmatrix} B^{\lambda_1,\lambda_2,\lambda_{12}}_{vj;v'j'}(R) \tag{9}$$

which is diagonal with respect to m_1 and m_2 and is independent of j_{12}. The 6D-CS potential matrix elements (8) reduce to the 5D-CS matrix elements (9) when $j_{12} = j'_{12} = 0$, and the 5D-CS matrix elements are easily related to the 4D-CS matrix elements given previously [20–22]. All dynamical formulations require the solution of a set of coupled equations of the form

$$\left[-\frac{\hbar^2}{2\mu}\frac{d^2}{dR^2} + \frac{\hbar^2 l(l+1)}{2\mu R^2} - E_c\right] F_n(R) + \sum_{n'} V_{n;n'}(R) F_{n'}(R) = 0 \tag{10}$$

where $E_c = E - E_n$. The CS approximation assumes that the off-diagonal elements of $\hat{l}^2$ with respect to Ω may be neglected, and the diagonal elements may be approximated by an effective orbital angular momentum quantum number $\bar{l}$ which replaces l in Eq. (10). Cross sections are given in terms of the appropriate T-matrix by

$$\sigma^{6D-CC}_{vj\to v'j'} = \frac{\pi}{(2j_1+1)(2j_2+1)2\mu E_c} \sum_{j_{12}j'_{12}ll'J} (2J+1) \left|T^J_{n;n'}(E_c)\right|^2, \tag{11}$$

$$\sigma^{6D-CS}_{vj\to v'j'} = \frac{\pi}{(2j_1+1)(2j_2+1)2\mu E_c} \sum_{j_{12}j'_{12}\bar{l}\Omega} (2\bar{l}+1) \left|T^{\bar{l}\Omega}_{n;n'}(E_c)\right|^2, \tag{12}$$

$$\sigma^{5D-CS}_{vj\to v'j'} = \frac{\pi}{(2j_1+1)(2j_2+1)2\mu E_c} \sum_{\bar{l}m_1m_2} (2\bar{l}+1) \left|T^{\bar{l}m_1m_2}_{n;n'}(E_c)\right|^2. \tag{13}$$

for the respective 6D-CC, 6D-CS, and 5D-CS formulations.

3. Results

All calculations were performed using a modified version of the TwoBC code [31] adapted to CO + H_2 with the 6D PES reported previously [19]. The radial coordinates of both molecules were represented as discrete variables with 20 points each. Gauss–Legendre quadratures were used for θ_1 and θ_2 with 14 points each, and a Gauss–Hermite quadrature was used for ϕ with 8 points. The maximum values for λ_1 and λ_2 were 10 and 6, respectively. The log-derivative matrix propagation method [32,33] was used to integrate the coupled equations from $R = 4 - 18$ a.u. in steps of 0.05 a.u. The maximum effective orbital angular momentum quantum number increased with collision energy and was given by $\bar{l}_{max} = 160$ for the highest energies considered. In all CS calculations, $\bar{l} \equiv J$ which is its average value between $J - j_{12}$ and $J + j_{12}$.

To assess the reliability of the CS calculations, we first benchmark the CS results against numerically exact CC results. Fig. 2 compares the total cross sections for vibrational quenching of CO(1,0) due to collisions with para-H_2(0,0) and ortho-H_2(0,1). In both cases, the basis set for the CO molecule included $j_1 = 0 - 40$ for $v_1 = 0$ and $j_1 = 0 - 20$ for $v_1 = 1$. The internal state of H_2 is restricted to the initial state, and the cross sections for the vibrational quenching of CO are summed over all rotational levels of $v'_1 = 0$. For para-H_2, the 5D-CS and 6D-CS results are identical and are compared against the 6D-CC results in the figure. Both formulations show sharp resonance structures in the $E_c = 1$–$10\ \mathrm{cm}^{-1}$ range, and the CC results show additional weaker structures for $E_c = 10$–$100\ \mathrm{cm}^{-1}$ which are missing in the CS results due to the larger energy steps used in the calculations. Both curves are smooth and in agreement with each other to within 30% for $E_c > 100\ \mathrm{cm}^{-1}$. The results are similar for ortho-H_2 collisions. For this case, the 5D-CS and 6D-CS results are not identical and are compared against the more accurate 6D-CC results. The CS results both show a broad shape resonance for $E_c < 1\ \mathrm{cm}^{-1}$ which is not present in the CC calculations. The agreement improves in the sharp resonance region ($\sim$1–10 cm^{-1}) although the agreement is only qualitative. The agreement with the CC calculations is generally better for the 6D-CS results. For $E_c > 100\ \mathrm{cm}^{-1}$, the 5D-CS and 6D-CS results converge and are in agreement with the CC results to within 40%. In both cases, the CS approximation is able to reproduce the main features of the cross sections. Rate coefficients for a Maxwellian velocity distribution are given in the Supplementary Information for the cross sections shown in Fig. 2.

Fig. 3 shows rotational level distributions of the cross sections for $\mathrm{CO}(1,0) \to \mathrm{CO}(0,j'_1)$ transitions due to collisions with $H_2(0,0)$ and $H_2(0,1)$ for three different collision energies. The distributions show the expected even/odd oscillations for $j'_1 < 10$ before falling off smoothly with increasing j'_1. These oscillations are due to the nearly homonuclear nature of CO and have been seen in H + CO collisions [34–36]. Fig. 3(a) and (c) show that the oscillations appear to be most prominent for the $\Omega = 0$ contribution. Fig. 3(c) and (d) show the agreement between the 5D-CS and 6D-CS approximations appears to be better at low j'_1 for $\Omega = 0$ and at high j'_1 for $\Omega = 1$. The $\Omega = 0$ and $\Omega = 1$ contributions are added together to obtain the total ortho-H_2 cross sections shown in Fig. 3(b). Comparison with Fig. 3(a) shows that the ortho and para cross sections are very similar for this special case where the H_2 basis set is restricted to a single state with no vibrational excitation.

Fig. 4 shows rotational level distributions of the cross sections for $\mathrm{CO}(1,0) \to \mathrm{CO}(v'_1,j'_1)$ transitions due to collisions with para-$H_2(0,0)$ for the three collision energies. The ortho-H_2 results are similar and are not shown. Cross sections obtained from 5D-CS and 6D-CC calculations are compared in the figure. Fig. 4(a) shows that there is some disagreement in the cross sections at $E_c = 10\ \mathrm{cm}^{-1}$, but the even/odd oscillations are present in both sets of calculations. The agreement improves as E_c increases to $100\ \mathrm{cm}^{-1}$. Fig. 4(b) shows cross sections for both $v'_1 = 0$ and $v'_1 = 1$ final states with $j'_2 = j_2 = 0$. The same curves are shown in Fig. 4(c) for $E_c = 1000\ \mathrm{cm}^{-1}$, and again the agreement between the two formulations is excellent. Fig. 4(d) shows that the agreement is not as good when the rotational state of H_2 changes to $j'_2 = 2$. In this case, the cross sections for the dominant CO rotational excitation transitions with $v'_1 = 1$ still show good

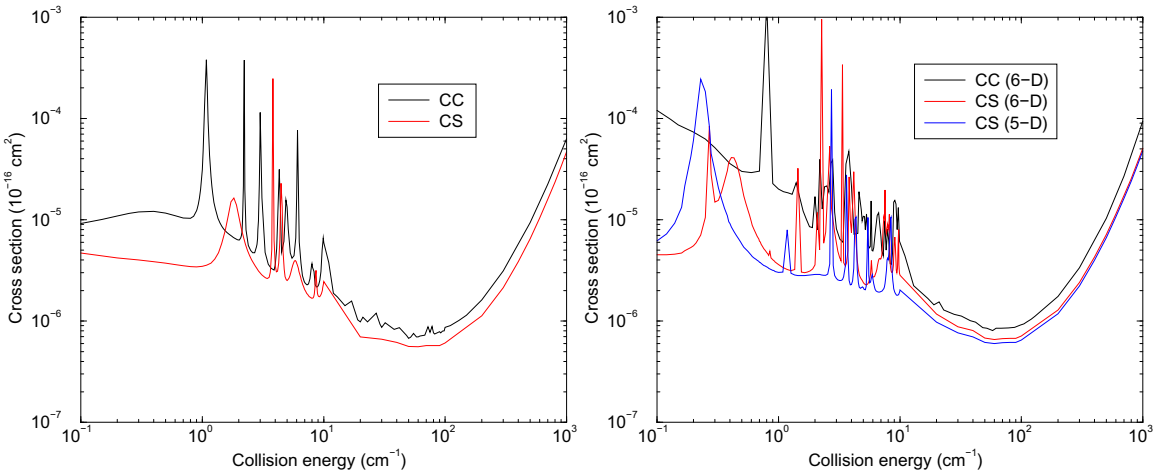

Fig. 2. Total cross sections for vibrational quenching of CO(1,0) due to collisions with H_2. The left panel is for H_2(0,0) and the right panel is for H_2(0,1). In both cases, the cross section is summed over all rotational levels of CO($v_1' = 0$) and the H_2 state is unchanged (ie., elastic).

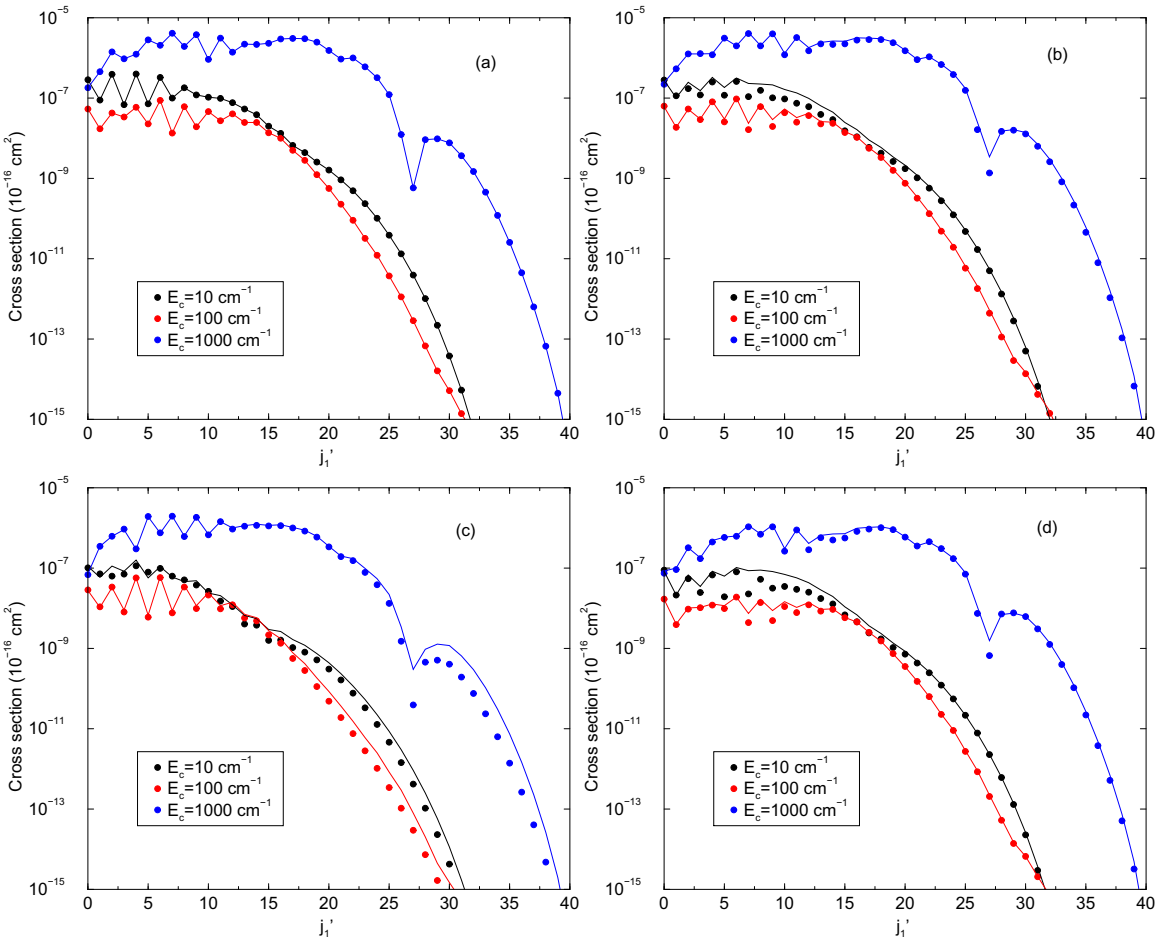

Fig. 3. Rotational level distributions for CO(1,0) + H_2($v_2 = 0$) cross sections for three different collision energies. Panels (a) and (b) correspond to para-H_2 and ortho-H_2 collisions, respectively. Panels (c) and (d) correspond to $\Omega = 0$ and $\Omega = 1$ contributions to the ortho-H_2 cross sections. In all cases, the final state is CO($0,j_1'$) and the H_2 state is unchanged. The points correspond to 5D-CS calculations and the solid lines correspond to 6D-CS calculations.

agreement. Cross sections for transitions to $v_1' = 0$ are in reasonable agreement for small j_1', however, the 5D-CS results tend to oscillate about the 6D-CC results at high j_1'. This result is consistent with previous studies [30] which found that angular momentum decoupling approximations tend to be less reliable when both molecules undergo a rotational change, especially when the transition involves a multi-quantum change in j. Fortunately, these transitions tend to be less efficient than other available transitions, so errors introduced by the approximation are reduced in significance. In general, we find that the 5D-CS approximation provides

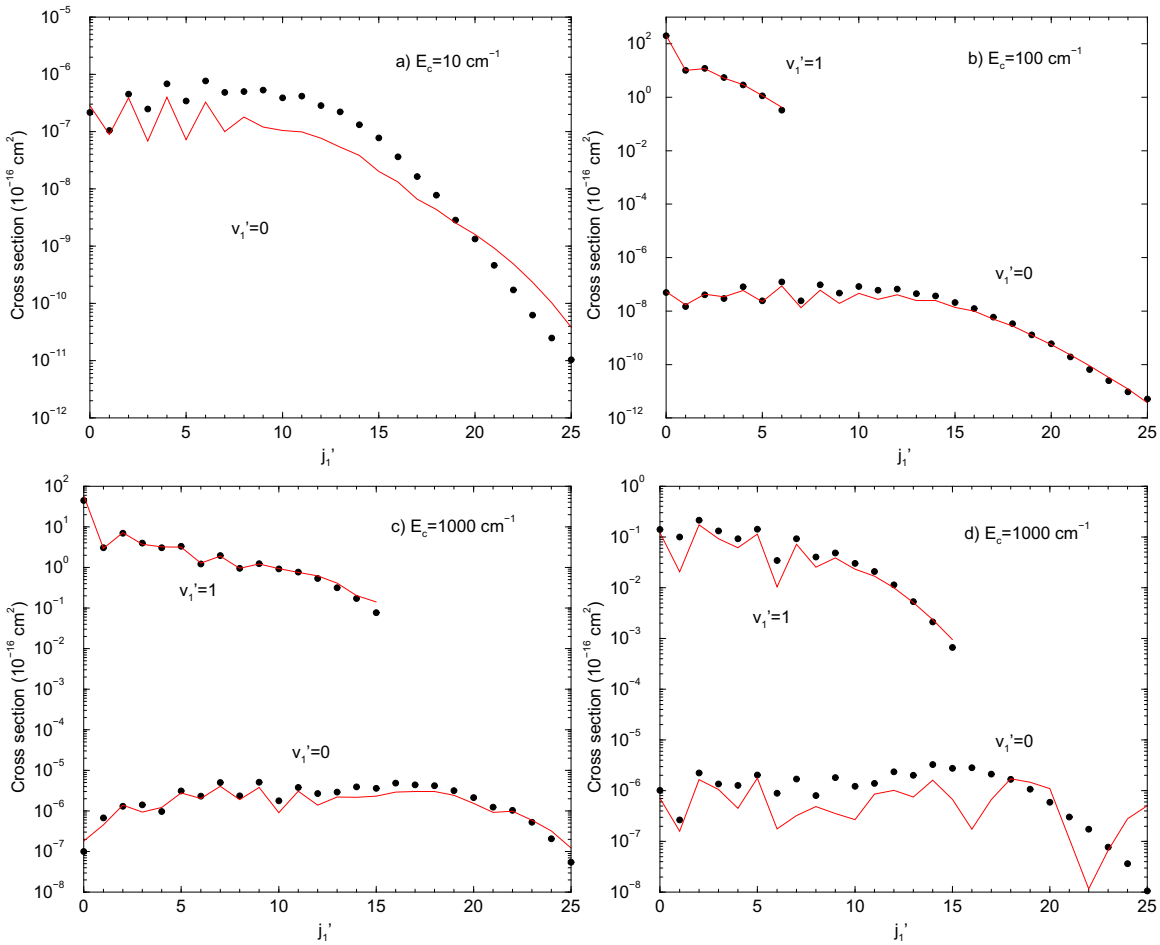

Fig. 4. Rotational level distributions for CO(1,0) + $H_2(0,0)$ cross sections. Panels (a), (b), and (c) correspond to the CO(v_1',j_1') + $H_2(0,0)$ final state at $E_c = 10$, 100, and 1000 cm^{-1}, respectively. Panel (d) corresponds to the CO(v_1',j_1') + $H_2(0,2)$ final state at $E_c = 1000$ cm^{-1}. For all panels, the points correspond to 6D-CC calculations and the solid red lines correspond to 5D-CS calculations. Note the changing cross section scale in each of the panels. (For interpretation of the references to color in this figure legend, the reader is referred to the web version of this article.)

an acceptable compromise between computational efficiency and accuracy.

The remaining results presented here are for collisions where both CO and H_2 are initially vibrationally excited. In this case, the basis sets are considerably larger than those where only one molecule is excited, and it is impractical to compute full CC cross sections. The 6D-CS formulation is also inefficient, and because it is not significantly more accurate than the 5D-CS approximation, we have opted to employ only the 5D-CS approximation over the energy range 10–10,000 cm^{-1}. The basis set for para-H_2 included $j_2 = 0-8$ for $v_2 = 0$ and $j_2 = 0-4$ for $v_2 = 1$. For ortho-H_2, the basis set included $j_2 = 1-9$ for $v_2 = 0$ and $j_2 = 1-5$ for $v_2 = 1$. For all calculations, the basis set for the CO molecule included $j_1 = 0-20$ for $v_1 = 0$ and $j_1 = 0-10$ for $v_1 = 1$. This CO basis set is considerably smaller than what was used to generate the results shown in Fig. 2. The reduced CO basis set allows efficient computation for the mutual vibrational quenching case using a modest computer workstation, however, it may introduce some basis set truncation error into the results at high collision energies (see Fig. 3).

Fig. 5 shows vibrational quenching cross sections for CO(1,0) due to para-$H_2(v_2 = 1)$ and ortho-$H_2(v_2 = 1)$. The cross sections are summed over all final state rotational levels of CO($v_1' = 0$). The curves shown in the figure correspond to vibrationally elastic collisions for the H_2 molecule. The curves are similar to those in Fig. 2 with minima near 100 cm^{-1} and smooth increases for higher energies. Cross sections for rovibrationally elastic $H_2(1,j_2)$ collisions are about 10 times larger than the rovibrationally elastic $H_2(0,j_2)$ cross sections shown in Fig. 2. The curves corresponding to rotational excitation of $H_2(v_2 = 1)$ show a similar shape to the $H_2(1,0)$ and $H_2(1,1)$ cross sections but are substantially smaller. For para-H_2, the curves show an orderly decrease for $H_2(1,0)$, $H_2(1,2)$, and $H_2(1,4)$ at all energies. For ortho-H_2, the pattern is not as orderly and there is a crossing of the $H_2(1,3)$ and $H_2(1,5)$ curves at $E_c = 400$ cm^{-1}.

Fig. 6 shows vibrational quenching cross sections for both CO and H_2 as a function of energy. The first thing to notice when both molecules undergo vibrational relaxation is the qualitatively different shape of the cross section curves. Whereas vibrationally elastic H_2 cross sections show minima near 100 cm^{-1} and a smooth increase with energy, the curves in Fig. 6 show a smooth decrease with energy before attaining minima near 600 cm^{-1}. This is due to the dominance of transitions which do not change the rotational state of H_2. Transitions to other $v_2' = 0$ levels of H_2 show an orderly decrease with j_2' on the low energy side of the minimum which span 5 orders of magnitude. At $E_c > 1000$ cm^{-1}, the curves converge to within an order of magnitude and the ordering of the curves is mixed. Fig. 7 shows vibrational quenching of H_2 accompanied by rotational excitation of CO($v_1 = 1$). The shape of the curves resemble those in Fig. 6 but are about 100 times larger in magnitude. The cross sections for para-$H_2(0,6)$ and $H_2(0,8)$ transitions are nearly identical, whereas the cross section for the ortho-

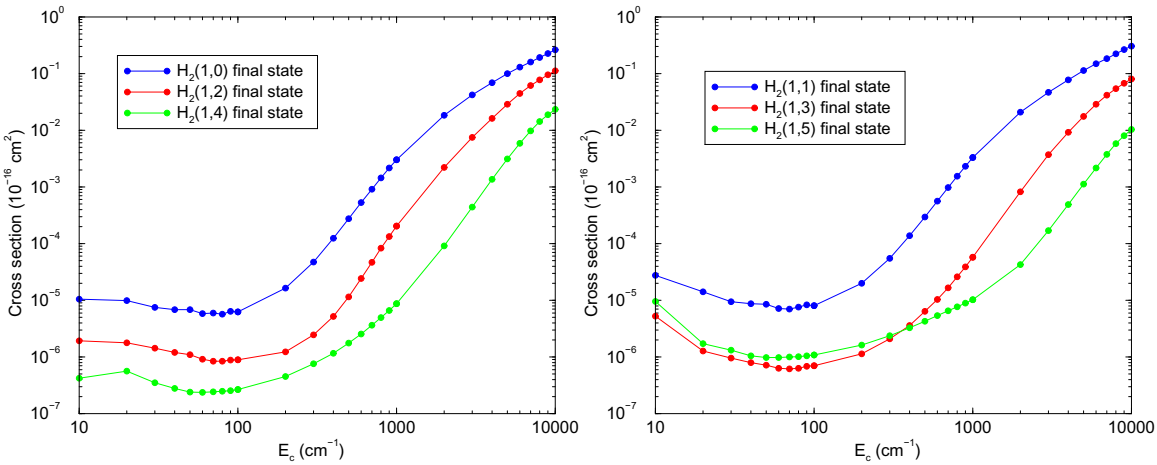

Fig. 5. Total cross sections for vibrational quenching of CO(1,0) due to collisions with H_2. The left panel is for H_2(1,0) and the right panel is for H_2(1,1). In both cases, the cross section is summed over all rotational levels of CO($v_1' = 0$) for the $H_2(v_2' = 1, j_2')$ final state.

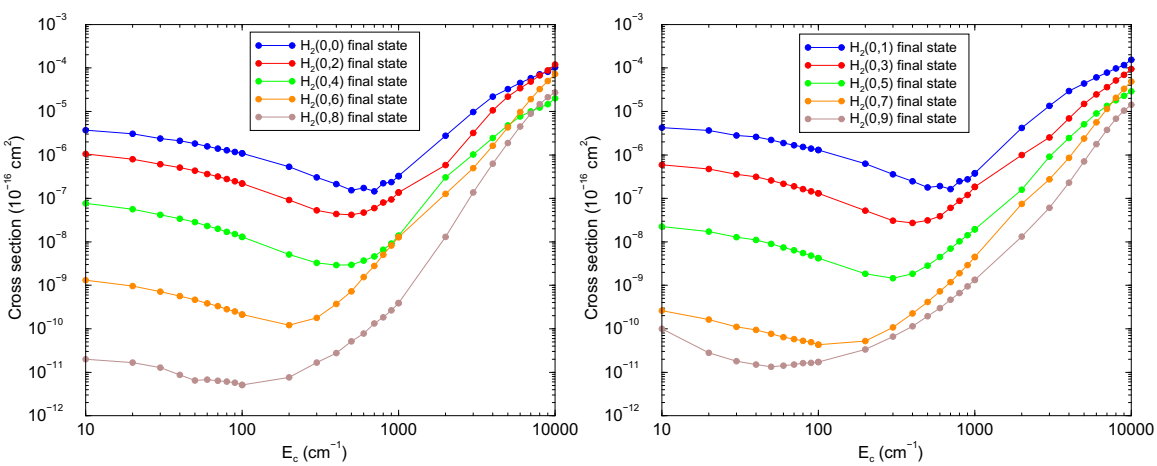

Fig. 6. Total cross sections for mutual vibrational quenching of CO(1,0) and H_2 due to collision. The left panel is for H_2(1,0) and the right panel is for H_2(1,1). In both cases, the cross section is summed over all rotational levels of CO($v_1' = 0$) for the $H_2(v_2' = 0, j_2')$ final state.

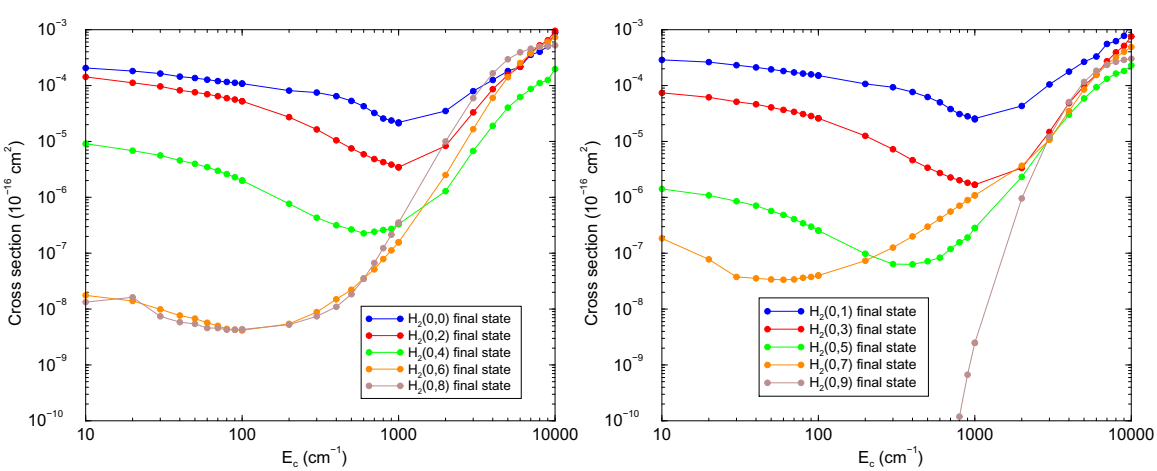

Fig. 7. Cross sections for rotational excitation of CO(1,0) and simultaneous vibrational quenching of $H_2(1, j_2)$. The left panel is for H_2(1,0) and the right panel is for H_2(1,1). The cross sections are summed over all excited rotational levels of CO($v_1' = 1$) for the designated $H_2(v_2' = 0, j_2')$ final state.

$H_2(0,7)$ transition is larger and crosses the $H_2(0,5)$ curve at about 200 cm^{-1}. The cross section for transition to $H_2(0,9)$ shows a channel threshold near 800 cm^{-1} but becomes comparable to the other curves near 3000 cm^{-1}.

Results for collisions which do not experience vibrational inelasticity are displayed in Fig. 8. As expected, the large rotational energy spacing for H_2 yields large differences in the rotational excitation cross sections for $H_2(v_2' = 1)$ with associated thresholds. The

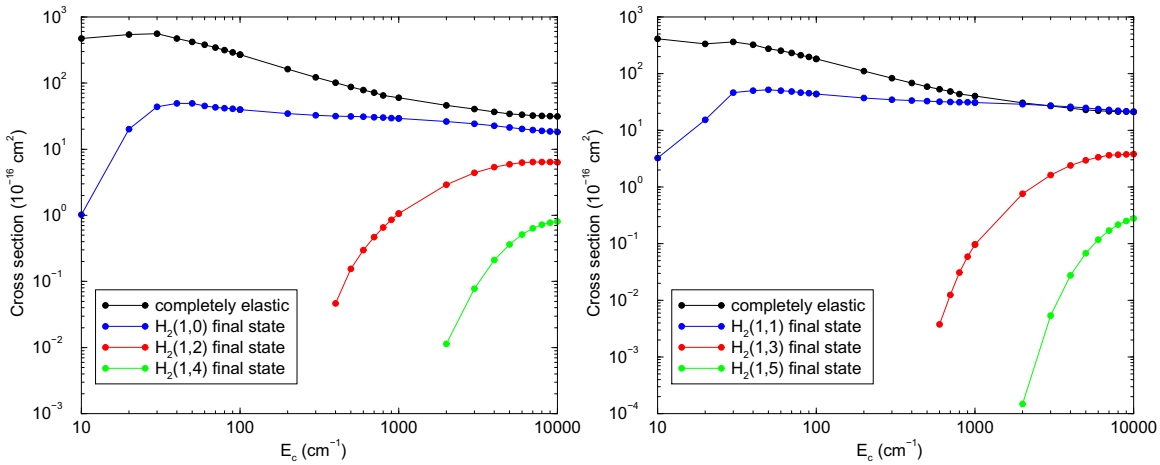

Fig. 8. Cross sections for completely elastic scattering and rotational excitation of CO(1,0) due to vibrationally elastic collisions with $H_2(1,j_2)$. The left panel is for H_2(1,0) and the right panel is for H_2(1,1). The excitation cross sections are summed over all excited rotational levels of CO($v_1' = 1$) for the designated $H_2(v_2' = 1, j_2')$ final state.

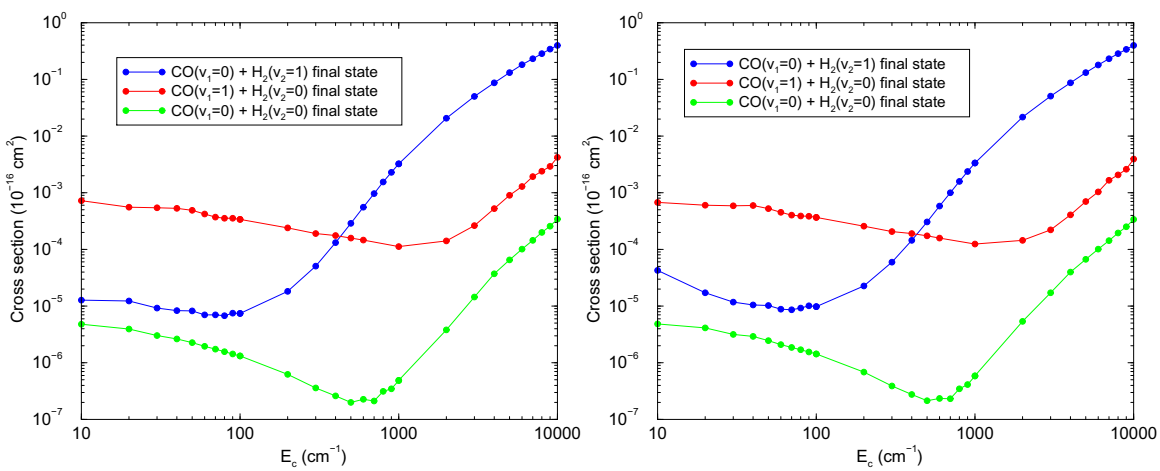

Fig. 9. Total cross sections for vibrational quenching of CO(1,0) and H_2 due to collision. The left panel is for H_2(1,0) and the right panel is for H_2(1,1). In both cases, the cross sections are summed over all final state rotational levels of both molecules.

small rotational energy spacing for CO yields curves for rotational excitation of CO that are comparable to the elastic case at high energy. For ortho-H_2, the summed cross section for rotational excitation of CO($v_1' = 1$) is identical to the completely elastic cross section for energies above 2000 cm^{-1}. For para-H_2, the summed cross section for rotational excitation of CO($v_1' = 1$) approaches the completely elastic cross section at high energy but is lower in magnitude. It is noteworthy that the difference in magnitude for rotational excitations of CO with and without vibrational de-excitation of H_2 is quite dramatic. The cross sections for the $H_2(1,0)$ final state in Fig. 8 are comparable to previous results [37] for rotational excitation of CO($v_1 = 0$) by $H_2(v_2 = 0)$. Pure rotational excitation cross sections for CO are expected to be very similar for $v_1 = 0$ and $v_1 = 1$ due to H_2, so this agreement may be an indirect validation of the 5D-CS approximation. Fig. 9 shows total cross sections for single and double vibrational de-excitations as a function of energy. It is interesting that vibrational quenching of H_2 dominates at low energy, whereas vibrational quenching of CO dominates at high energy. The behavior at high energy is due to the difference in the vibrational energy gaps (2144.7 cm^{-1} for CO and 4161 cm^{-1} for H_2) which suggests that CO should quench preferentially. At low energy, the situation is reversed due to the greater anisotropy in the PES for stretching of H_2 compared to CO. The cross-over for both ortho and para occurs at $E_c \sim 400$ cm^{-1} which is just below where the double vibrational de-excitation curves show a minimum. The vibrational quenching efficiency of H_2 is about 80 times greater than for CO at $E_c = 10$ cm^{-1} and about 100 times smaller than for CO at $E_c = 10,000$ cm^{-1}. The ratio of single to double vibrational quenching ranges from 200 at low energies to 1000 at high energies.

4. Conclusions

Mutual vibrational quenching of CO and H_2 is a challenging computational problem for quantum mechanical scattering formulations. The closely spaced rotational levels for CO lead to substantial internal angular momentum coupling between the molecules. Additional angular momentum coupling arises when orbital angular momentum is properly taken into account within the numerically exact CC formulation. Recent 6D-CC calculations [19] required substantial computational effort for the case of vibrationally excited CO with H_2 restricted to its vibrational ground state. The computational demands would further increase with the inclusion of additional vibrational flexibility in the basis sets. Therefore, it is necessary to find an alternative formulation for

studying the mutual vibrational quenching of CO and H_2. The CS approximation generally offers the best compromise between accuracy and computational effort. In this approximation, the exact orbital angular momentum quantum number is replaced by an effective value which allows substantial decoupling, particularly at high collision energies. The potential matrix elements are diagonal with respect to the total angular momentum projection quantum number. Off-diagonal coupling between states with different projection quantum numbers are neglected in the 6D-CS approximation, and if the twist-angle dependence of the PES is also neglected, a 5D-CS approximation is achieved. The CS approximation predicts cross sections for single vibrational quenching that are about 200–1000 times larger than mutual vibrational quenching for $E_c = 10{-}10,000\ \mathrm{cm}^{-1}$. The vibrational quenching efficiency of CO is greater than H_2 at high energies and smaller at low energies, and the vibrational quenching efficiencies are approximately equal at 400 cm^{-1}.

The present results for CO($v_1 = 1$) collisions with vibrationally excited para-H_2($v_2 = 1$) and ortho-H_2($v_2 = 1$) suggest that a viable means for computing a full database of quantum mechanical cross sections and rate coefficients is within reach. A database of this type is urgently needed for accurate modeling of astrophysical environments which are currently limited to scaling techniques. Because the database would be largely comprised of theoretical calculations which use a dynamical decoupling approximation and reduced dimensionality, it is essential to benchmark wherever possible. Previously, it was demonstrated that quantum dynamics of CO + H_2 in full dimensionality provides good agreement with experiment [19] in the limited cases where experimental data are available. Here, we use the existing 6D-CC results to benchmark the CS approximation. The 6D-CS formulation is also inefficient, and because it is not significantly more accurate than the 5D-CS approximation, we have opted to employ only the 5D-CS approximation over the energy range 10–10,000 cm^{-1}. Based on the comparisons and previous experience with H_2-H_2 [30], we conservatively estimate that the results are reliable to within 50% for most transitions and give the correct trends in the relative cross sections. A full database of such cross sections and associated rate coefficients would add to existing rotational quenching data [38] and provide an invaluable tool for astrophysical models .

Conflict of interest

There is no conflict of interest to declare.

Acknowledgments

This work was supported at Penn State by NSF Grant No. PHY-1203228, at UGA by NASA Grant NNX12AF42G, and at UNLV by NSF Grant No. PHY-1205838.

Appendix A. Supplementary data

Supplementary data associated with this article can be found, in the online version, at http://dx.doi.org/10.1016/j.chemphys.2015.07.001. These data include MOL files and InChiKeys of the most important compounds described in this article.

References

[1] W.J. Hooker, R.C. Millikan, J. Chem. Phys. 38 (1963) 214.
[2] R.C. Millikan, L.A. Osburg, J. Chem. Phys. 41 (1964) 2196.
[3] D.J. Miller, R.C. Millikan, J. Chem. Phys. 53 (1970) 3384.
[4] A.J. Andrews, C.J.S.M. Simpson, Chem. Phys. Lett. 36 (1975) 271.
[5] A.J. Andrews, C.J.S.M. Simpson, Chem. Phys. Lett. 41 (1976) 565.
[6] G.J. Wilson, M.L. Turnidge, A.S. Solodukhin, C.J.S.M. Simpson, Chem. Phys. Lett. 207 (1993) 521.
[7] B.T. Draine, F. Bertoldi, Astrophys. J. 468 (1996) 269.
[8] D.J. Hollenbach, A.G.G.M. Tielens, Rev. Mod. Phys. 71 (1999) 173.
[9] E.F. van Dishoeck, J.H. Black, Astrophys. J 334 (1998) 771.
[10] S. Warin, J.J. Benayoun, Y.P. Viala, A&A 308 (1996) 535.
[11] F. Le Petit, C. Nehme, J. Le Bourlot, E. Roueff, Astrophys. J. Suppl. Ser. 164 (2006) 506.
[12] M. Röllig et al., A&A 467 (2007) 187.
[13] G. Shaw, G.J. Ferland, N.P. Abel, P.C. Stancil, P.A.M. van Hoof, Astrophys. J. 624 (2005) 794.
[14] R.E. Lupu, P.D. Feldman, H.A. Weaver, G.-P. Tozzi, Astrophys. J. 670 (2007) 1473.
[15] M.R. Swain et al., Astrophys. J. Lett. 690 (2009) L114–L117.
[16] D. Narayanan et al., Astrophys. J. Suppl. Ser. 174 (2008) 1330.
[17] K.M. Walker, B.H. Yang, P.C. Stancil, N. Balakrishnan, R.C. Forrey, Astrophys. J. 790 (2014) 96.
[18] T.V. Tscherbul, Chem. Phys. Lett. 393 (2004) 58.
[19] B.H. Yang, P. Zhang, X. Wang, P.C. Stancil, J.M. Bowman, N. Balakrishnan, R.C. Forrey, Nat. Commun. 6 (2015) 6629.
[20] Z. Bačić, R. Schinke, G.H.F. Diercksen, J. Chem. Phys. 82 (1985) 236.
[21] Z. Bačić, R. Schinke, G.H.F. Diercksen, J. Chem. Phys. 82 (1985) 245.
[22] J.P. Reid, C.J.S.M. Simpson, H.M. Quiney, J. Chem. Phys. 106 (1997) 4931.
[23] D.R. Flower, Mon. Not. R. Astron. Soc. 425 (2012) 1350.
[24] R.T. Pack, J. Chem. Phys. 60 (1974) 633.
[25] P. McGuire, D.J. Kouri, J. Chem. Phys. 60 (1974) 2488.
[26] P. McGuire, J. Chem. Phys. 62 (1975) 525.
[27] S. Green, J. Chem. Phys. 62 (1975) 2271.
[28] M.H. Alexander, A.E. DePristo, J. Chem. Phys. 66 (1977) 2166.
[29] T.G. Heil, S. Green, D.J. Kouri, J. Chem. Phys. 68 (1978) 2562.
[30] A. Bohr, S. Paolini, R.C. Forrey, N. Balakrishnan, P.C. Stancil, J. Chem. Phys. 140 (2014) 064308.
[31] R.V. Krems, TwoBC – Quantum Scattering Program, University of British Columbia, Vancouver, Canada, 2006.
[32] B.R. Johnson, J. Comput. Phys. 13 (1973) 445.
[33] D.E. Manolopoulos, J. Chem. Phys. 85 (1986) 6425.
[34] K.T. Lee, J.M. Bowman, J. Chem. Phys. 886 (1987) 215.
[35] S.D. Augustin, W.H. Miller, Phys. Lett. 28 (1974) 149.
[36] S. Chapman, S. Green, J. Chem. Phys. 67 (1977) 2317.
[37] B.H. Yang, P.C. Stancil, N. Balakrishnan, R.C. Forrey, J. Chem. Phys. 124 (2006) 104304.
[38] B.H. Yang, P.C. Stancil, N. Balakrishnan, R.C. Forrey, Astrophys. J. 718 (2010) 1062.